Time-Lagged Response of the Antarctic and High-Latitude Atmosphere to Tropical MJO Convection

GINA R. HENDERSON, BRADFORD S. BARRETT, ASHLEY LOIS, AND HAADI ELSAAWY

Oceanography Department, U.S. Naval Academy, Annapolis, Maryland

(Manuscript received 2 August 2017, in final form 22 February 2018)

ABSTRACT

Intraseasonal tropical variability has important implications for the mid- and high-latitude atmosphere, and in recent studies has been shown to modulate a number of weather processes in the Northern Hemisphere, such as snow depth, sea ice concentration, precipitation, atmospheric rivers, and air temperature. In such studies, the extratropical atmosphere has tended to respond to the tropical convection of the leading mode of intraseasonal variability, the Madden–Julian oscillation (MJO), with a time lag of approximately 7 days. However, the time lag between the MJO and the Antarctic atmosphere has been found to vary between less than 7 and greater than 20 days. This study builds on previous work by further examining the time-lagged response of Southern Hemisphere tropospheric circulation to tropical MJO forcing, with specific focus on the latitude belt associated with the Antarctic Oscillation, during the months of June (austral winter) and December (austral summer) using NCEP–DOE Reanalysis 2 data for the years 1979–2016. Principal findings indicate that the time lag with the strongest height anomalies depends on both the location of the MJO convection (e.g., the MJO phase) and the season, and that the lagged height anomalies in the Antarctic atmosphere are fairly consistent across different vertical levels and latitudinal bands. In addition, certain MJO phases in December displayed lagged height anomalies indicative of blocking-type atmospheric patterns, with an approximate wavenumber of 4, whereas in June most phases were associated with more progressive height anomaly centers resembling a wavenumber-3-type pattern.

1. Introduction

Weather patterns have traditionally spanned time scales from subdaily up to biweekly, and climate patterns have spanned time scales from seasonal to multidecadal and beyond. The period between the biweekly and seasonal, known as the intraseasonal time scale, acts as a bridge between weather and climate (Jones et al. 2015), and it includes phenomena such as the tropical Madden–Julian oscillation (MJO; Madden and Julian 1972) and many extratropical teleconnections (Wallace and Gutzler 1981). The convectively active phase of the MJO manifests itself as a region of eastward-propagating large-scale convective cloud clusters approximately 10 000 km in horizontal extent that typically initiate in the tropical Indian Ocean, move eastward across the Maritime Continent, and dissipate in the tropical Pacific Ocean. On either side of this region of enhanced convection are regions of suppressed convection, connected to the enhanced convection by overturning tropospheric circulation cells. A Rossby wave teleconnection to the extratropics forms as a consequence of the diabatic heating in the tropical upper troposphere produced by the MJO convective region (Hoskins and Karoly 1981; Sardeshmukh and Hoskins 1988; Ferranti et al. 1990; Bladé and Hartmann 1995; Jin and Hoskins 1995; Seo and Son 2012). This teleconnection yields profound associations between the MJO and the extratropics (Roundy 2012; Zhang 2013). Indeed, the character of mid- and high-latitude weather at lead times longer than approximately 5 days can be greatly influenced by the temporal and geographic evolution of MJO convection in the tropics (Weickmann et al. 1997; Mo and Higgins 1998a; Hendon et al. 2000; Paegle et al. 2000; Mo 2000; Branstator 2002; Jones et al. 2004; Weickmann and Berry 2007; Schreck et al. 2013). Of particular focus for this study is the potential for associations between the MJO and weather patterns in the extratropical Southern Hemisphere.

Given its connections with extratropical circulation, much attention has been given recently to the interaction between the MJO and many of the leading modes of extratropical variability. For the Northern Hemisphere, the MJO is known to associate with the polarity of the North Atlantic Oscillation (Cassou 2008), the

Corresponding author: Dr. Gina R. Henderson, ghenders@usna.edu

DOI: 10.1175/MWR-D-17-0224.1

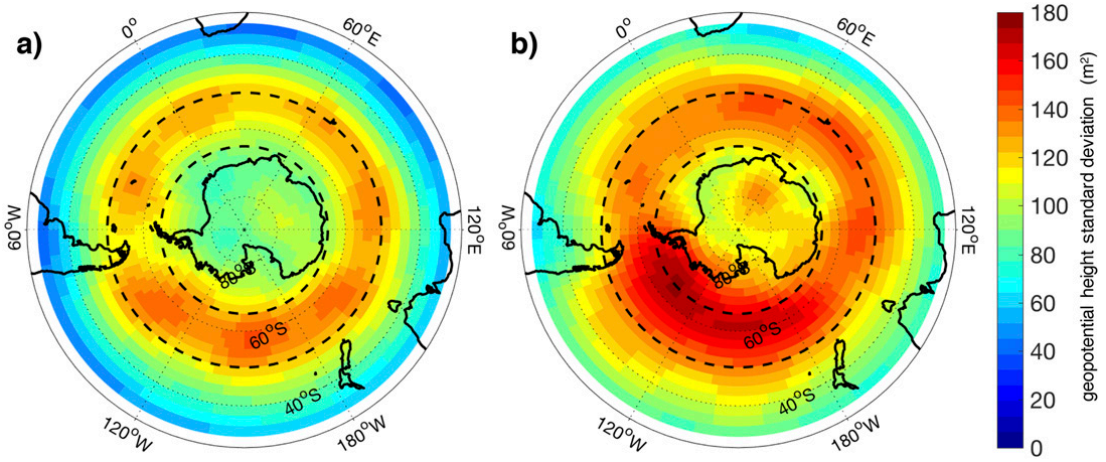

FIG. 1. Standard deviation of 500-hPa geopotential height (m) for (a) June and (b) December for the years 1979–2016. Latitudinal band from 50° to 65°S is indicated between black dashed lines.

Arctic Oscillation (Zhou and Miller 2005; L'Heureux and Higgins 2008), and the Pacific–North American pattern (Schreck et al. 2013), as well as flow blocking patterns around Greenland (Henderson et al. 2016) and the North Pacific (Moore et al. 2010). Indeed, via its interaction with large-scale circulation, the MJO has been shown to modulate a number of weather processes in the Northern Hemisphere, such as snow depth (Guan et al. 2012; Barrett et al. 2015; Li et al. 2016), sea ice concentration (Henderson et al. 2014), precipitation (Donald et al. 2006), atmospheric rivers (Higgins et al. 2000), and air temperature (Vecchi and Bond 2004; Seo et al. 2016; Zhou et al. 2016).

Similar attention has been given to important interactions between the MJO and leading modes of variability of the Southern Hemisphere atmosphere. Tropical convection between the Indian Ocean and Australia can force a wave train extending eastward and poleward across the Pacific, reaching South America (Kiladis and Weickmann 1992a,b; Berbery and Nogues-Paegle 1993; Kiladis and Weickmann 1997; Mo and Higgins 1998b). These Rossby waves generated by tropical MJO convection are responsible for observed intraseasonal variability in the meridional wind component at 500 hPa over the southeast Pacific (Renwick and Revell 1999) and summer precipitation (Paegle et al. 2000) and temperature (Jacques-Coper et al. 2015) over South America. Surface westerly winds around almost the entire 60°S latitude circle accelerate during austral winter (JJA) approximately 7 days after anomalous MJO convection peaks in the Indian Ocean (Matthews and Meredith 2004). That variability is connected to the southern annular mode (SAM; Limpasuvan and Hartmann 1999), and results in a maximum in circumpolar ocean transport 3 days after the peak in the SAM. Furthermore, negative Antarctic Oscillation (AAO; Sun et al. 2017; Gong and Wang 1998, 1999) events are associated with tropical convection in the tropical Pacific Ocean. Both El Niño and eastward-propagating MJO events (Sobel and Maloney 2013) can excite negative AAO occurrences during austral summer (DJF) as poleward-propagating Rossby waves decrease 700-hPa heights around 45°S and increase 700-hPa heights over Antarctica (Carvalho et al. 2005). Indeed, a relationship exists between the MJO and austral winter (JJA) midtroposphere circulation and accumulated precipitation in Chile (Barrett et al. 2012), although that study did not examine time lags. Those lags were examined to connect the MJO to dominant weather regimes over New Zealand, although substantial variability exists in the time lag between tropical MJO convection and the extratropical signal (Fauchereau et al. 2016). For example, some of the strongest time-lagged responses in the extratropical geopotential height field were seen 15–20 days after MJO active convection, suggesting that better understanding and predictions of MJO could lead to improvements in weather predictability on those time scales.

This current study builds on those previous results by examining the time-lagged evolution of Southern Hemisphere tropospheric circulation with active MJO events. The specific focus here is in the mid- to high latitudes, in the latitude belt associated with strongest variability of the AAO (Fig. 1). The primary objective of this study is to examine the concomitant evolution of the midlatitude response, illustrated by extratropical height anomalies, under different phases of the MJO. This time lag has been suggested at 7–10 days between the AAO and the MJO, with AAO polarity responding most strongly 7–10 days after MJO convection (Flatau and Kim 2013), and out to 20 days between MJO convection and extratropical circulation (Fauchereau et al. 2016). We focus on differences in time lags between austral summer (DJF, when the MJO is most convectively intense;

Lafleur et al. 2015) and austral winter (JJA, when extratropical circulation is strongest in the Southern Hemisphere). The remainder of this paper is organized as follows: data and methodology are presented in section 2, results are presented in section 3, and a discussion and the conclusions are presented in section 4.

2. Data and methodology

The analyses in this study were based on two publicly available datasets. First, the intensity and position of the MJO was determined according to the daily Real-time Multivariate MJO (RMM) index (Wheeler and Hendon 2004; http://www.bom.gov.au/climate/mjo/). The RMM index divides the MJO into eight phases, each one corresponding to a broad geographic location of the MJO's enhanced equatorial convective signal derived from 850- and 200-hPa zonal wind and outgoing longwave radiation. The index is designed such that the oscillation generally progresses eastward as phase number increases, from phase 1 to 8 and back to phase 1 again. For this study, days when the RMM amplitude was greater than 1.0 were classified as "active" MJO days, while days during which the RMM magnitude was less than or equal to 1.0 were classified as "inactive" MJO days and were referred to as "phase 0." It is important to note that the RMM index is not without limitations. For example, the use of a single pair of EOFs helps provide simplicity, but it cannot capture subtle differences of every MJO event, which evolve with varying structures (Ventrice et al. 2013). Furthermore, higher-frequency noise may also be present in the index as a result of the lack of a bandpass time filter (Roundy et al. 2009). Additionally, the RMM index relies on large-scale circulation patterns for MJO detection and may not detect MJO initiation when these signals are absent (Straub 2013). Last, meridional averaging of OLR signals may pose difficulty in detecting MJO shifts across hemispheres (Ventrice et al. 2011). Despite these limitations, the RMM index has been successfully used in multiple other studies to identify modulations in the extratropical atmosphere [see reviews by Zhang (2005, 2013)], and here we use the RMM to classify the large-scale character of the MJO.

Second, atmospheric data were obtained from the National Centers for Environmental Prediction–Department of Energy (NCEP–DOE) Reanalysis 2 (Kanamitsu et al. 2002; https://www.esrl.noaa.gov/psd/data/gridded/data.ncep.reanalysis2.html). Daily values of 300-, 500-, and 700-hPa geopotential heights for the period 1979–2016 were analyzed. Daily composite anomalies of geopotential height at those three atmospheric levels were calculated for both winter and summer by phase of the active MJO. Daily geopotential heights were converted to standard anomalies by subtracting the long-term (1979–2016) mean for the 31-day period centered on each day, and then dividing that anomaly by the long-term (1979–2016) standard deviation for the same 31-day period. Those daily standard anomalies were then binned by RMM phase and averaged. Anomalies for each MJO phase were tested for statistical significance using a two-tailed Student's t test at each grid point, with the null hypothesis that there was no difference between active MJO and the long-term mean, following the methodology of Barrett et al. (2015). Anomalies that were statistically significant at the 95% confidence level were retained. Finally, results from June and December are presented, as they are representative of conditions in austral winter and summer, respectively.

To assess temporal lags between the MJO and the Antarctic atmosphere, standard absolute anomalies (SAAs) were calculated by dividing the absolute value of the daily anomaly (calculated as above) by the standard deviation. Statistically significant SAAs were then binned by MJO phase and averaged over 5 different latitudinal bands (across all longitudes), to assess the association between the Antarctic atmosphere in a particular latitudinal band to MJO at time lags from 0 to 30 days after MJO convection. To prevent overweighting of the higher latitudes (whose grid points cover less area), a weighting function $\cos(\theta)$, where θ is the latitude of the grid point, was applied to each height anomaly. The analysis primarily focuses on the 50°–65°S latitudinal band, as the geopotential heights in that band have the largest variance in both June and December (Mo 2000) (Fig. 1). To investigate sensitivity of the MJO–Antarctic atmosphere relationship, four other latitudinal bands were also analyzed: 45°–65°S, 55°–65°S, 55°–70°S, and 55°–80°S, and anomalies in those bands were weighted by latitude using the method described above. Finally, height anomalies in each latitudinal band and at each pressure level were separated into their positive and negative components for each phase to assess the extent to which the height anomalies are evenly distributed at each lag and MJO phase, or if there is a tendency for more positive or negative height anomalies.

3. Results

a. *Lag association between MJO and the Antarctic atmosphere*

To assess the temporal lag in geopotential heights in the Antarctic region after an active MJO event, the latitudinal band of 50°–65°S first was considered. During June (austral winter), positive and negative standard anomalies of lagged 500-hPa geopotential height for all MJO phases reveal a slowly evolving association with the atmosphere, with differences noted for both MJO phase and lag duration (Fig. 2). For example, after active MJO phase-8 occurrences (when MJO convection is

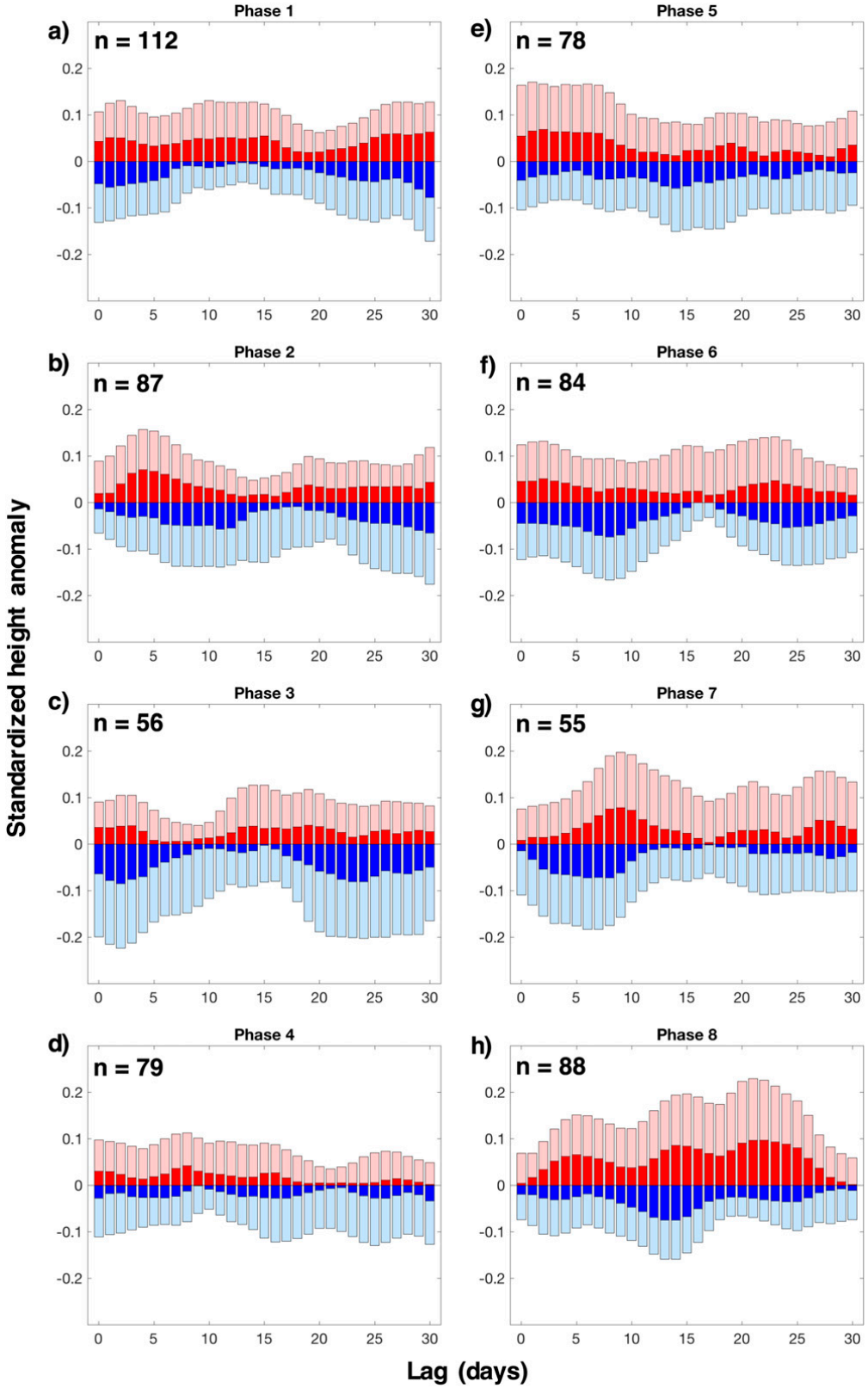

FIG. 2. Mean positive (red bars) and negative (blue bars) 500-hPa geopotential height standard anomalies (in nondimensional units) at 0–30-day temporal lags for MJO phases (a) 1, (b) 2, (c) 3, (d) 4, (e) 5, (f) 6, (g) 7, and (h) 8 for June, for the years 1979–2016. Standard anomalies are averaged across the latitudinal band 50°–65°S. Darker shading indicates anomalies that are statistically significant at the 95% confidence level. Sample size (days) is indicated for each composite.

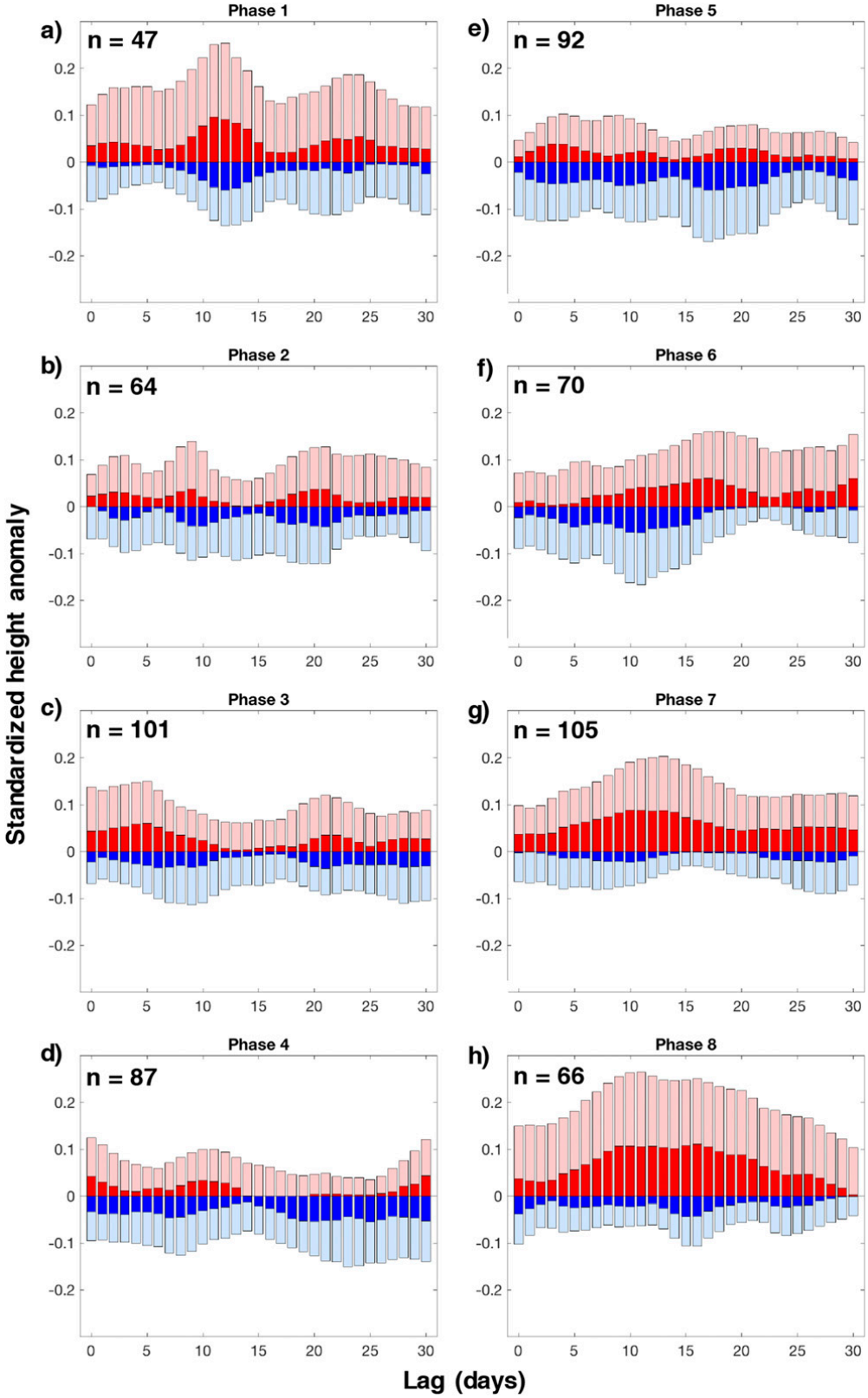

FIG. 3. As in Fig. 2, but for December.

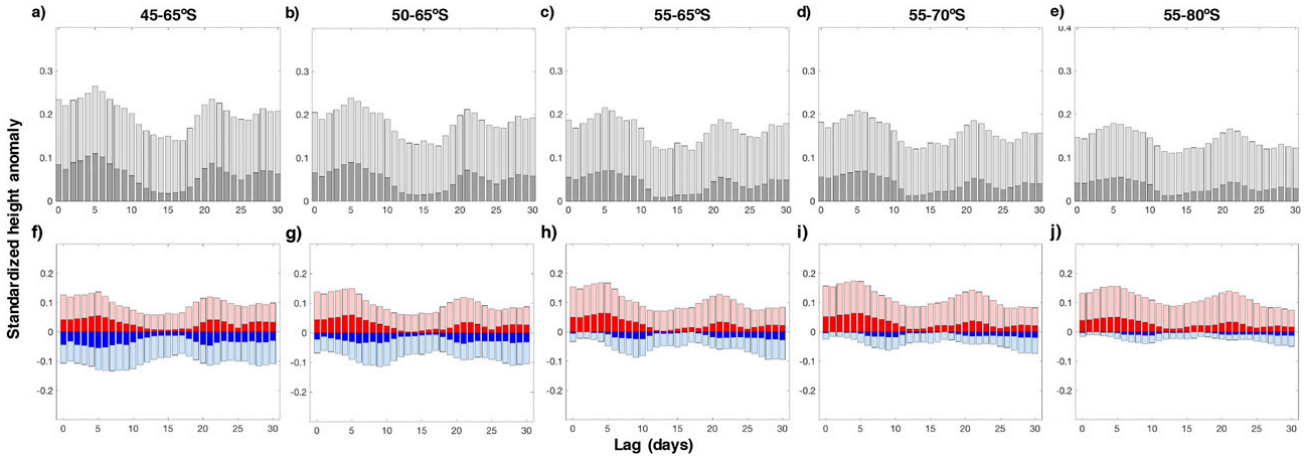

FIG. 4. (a)–(e) Mean standard absolute anomalies and (f)–(j) positive and negative standard anomalies of 500-hPa geopotential height (in nondimensional units) for all latitudinal bands (45°–65°S, 50°–65°S, 55°–65°S, 55°–70°S, and 55°–80°S) at 0–30-day temporal lags for MJO phase 3 in December. Darker shading indicates anomalies that are statistically significant at the 95% confidence level.

over the Western Hemisphere), the Antarctic atmosphere tends to be dominated by positive height anomalies at nearly all temporal lags from 0 to 30 days (Fig. 2h). In contrast, height anomalies concurrent with and after MJO phase-3 events (when MJO convection is over the Indian Ocean) tend toward more negative anomalies (Fig. 2c). For some phases, greater magnitude negative (positive) height anomalies tend to lead (lag) similar increase magnitude anomalies in the opposite sign, as can be seen from the positive anomalies 5 days after phase 2 (when MJO convection is over the Indian Ocean), that subsequently weaken and turn more negative by 10 days after phase 2 (Fig. 2b). This pattern again can be seen after phase 7 (when MJO convection is over the western Pacific), with negative anomalies 5–7 days after phase 7 that weaken and turn more positive by 10 days after phase 7 (Fig. 2g).

For all MJO phases in June, the atmosphere tends toward both positive and negative height anomalies in the 50°–65°S latitudinal band. The time lag associated with the largest magnitude height anomalies varies by phase, with some phases have multiple peak lags for both positive and negative standard anomalies. For example, a peak in height anomalies occurs approximately 5 days after MJO phase-8 events (when the MJO is active over the Western Hemisphere), with another peak evident around 22 days (Fig. 2h). Phases 6 and 7 (when MJO convection is over the western Pacific) both show peaks in negative anomalies approximately 7–9 days after active occurrences of each respective phase (Figs. 2f,g). In contrast, phase 4, when MJO convection is over the Maritime Continent, tends toward smaller-magnitude lags, with few peaks in either positive or negative height anomalies (Fig. 2d).

When considering time lags of the 500-hPa height field between 50° and 65°S during December (austral summer), a similar story emerges: the most important time lags tend to vary by phase (Fig. 3). In contrast to June, standard anomalies tend to be positive after phase-7, -8, and -1 events (when MJO is active over the western Pacific into the Western Hemisphere), with a consistent peak in positive anomalies 10–15 days after those phases (Figs. 2g, 2h, and 2a). After phase 5, height anomalies tend to be smaller in magnitude and predominately negative (Fig. 3e), which is a different anomaly pattern than after the same phase in June (Fig. 2e). Antarctic height anomalies after MJO phase-2 and -3 events (when MJO convection is over the Indian Ocean) tend to be equally distributed between positive and negative values, displaying smaller anomaly magnitudes than all other phases during this month. After phase 4, height anomalies are more negative than positive at all time lags out to 30 days. The differences between summer and winter association between MJO and the Antarctic atmosphere is likely, at least in part, because of seasonality of the MJO itself (stronger convection in austral summer, weaker in winter), and of seasonality of the state of the Antarctic atmosphere (stronger and equatorward-displaced circulation in austral winter, weaker and poleward-displaced circulation in summer).

b. Spatial dependence of lagged Antarctic heights

The next step toward better understanding the spatial variability of the Antarctic atmosphere in the 30 days after MJO convection is to consider anomalies of 500-hPa geopotential height for all temporal lags from 0 to 30 days in four additional latitudinal bands: 45°–65°S,

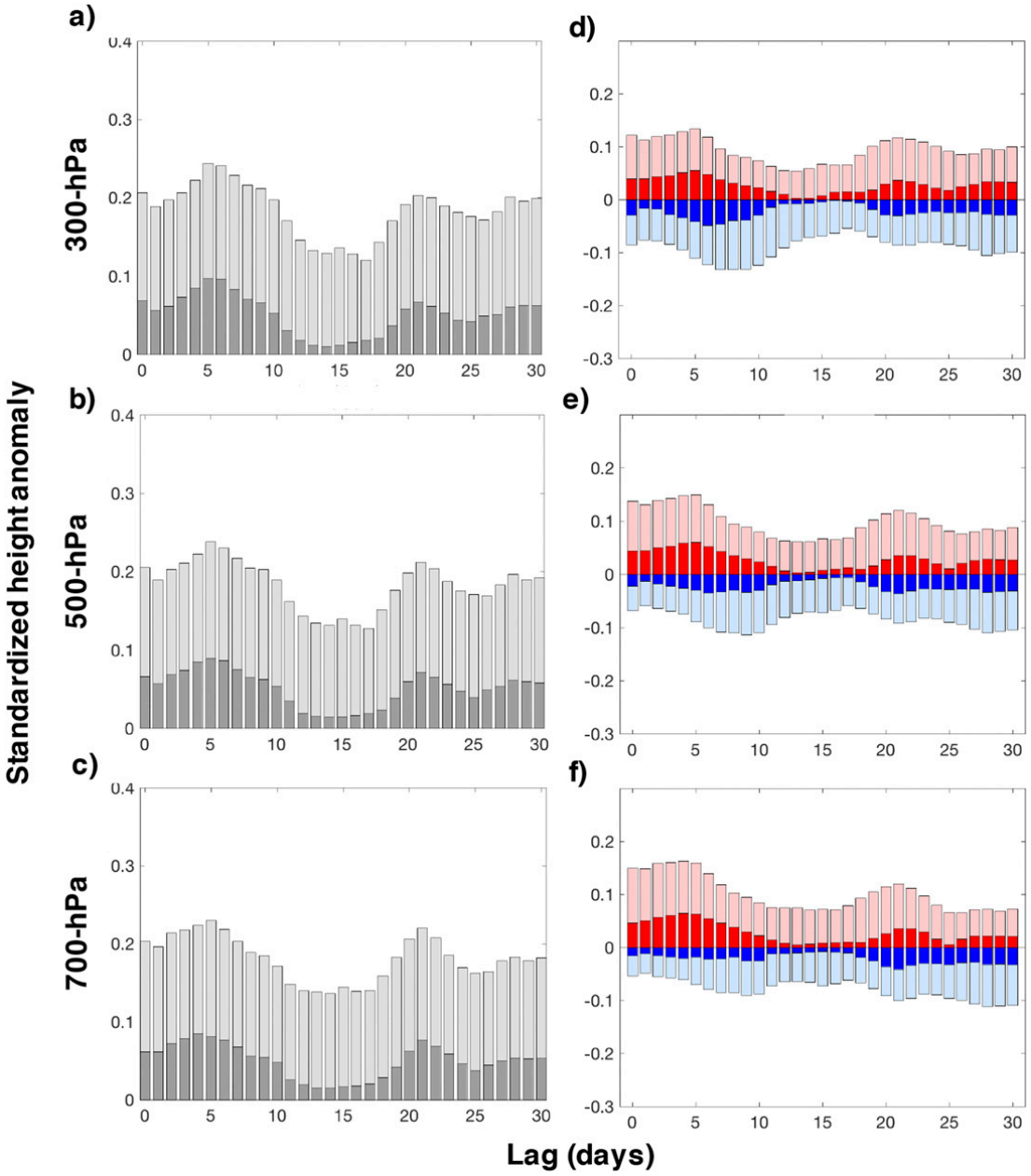

FIG. 5. (a)–(c) Mean standard absolute anomalies and (d)–(f) positive and negative standard anomalies of 300-, 500-, and 700-hPa geopotential height (in nondimensional units) at 0–30-day temporal lags for MJO phase 3 in December. Standard anomalies are for the latitudinal band 50°–65°S. Darker shading indicates anomalies that are statistically significant at the 95% confidence level.

55°–65°S, 55°–70°S, and 55°–80°S. Results in this subsection are presented for December phase 3 (when MJO convection is in the Indian Ocean) (Fig. 4). Phase 3 was chosen somewhat arbitrarily, as the other seven phases in December behave similarly. Anomalies at all lags for the five different latitudinal bands (Fig. 4, top row) tend to be largely insensitive to latitudinal band size or location, although as successively higher latitudes are included, the anomalies tend to be more positive (Figs. 4h–j). This observation is demonstrated by consistent peaks in anomalies around 5 and 20 days after MJO convection for all latitudinal bands (Figs. 4a–e). Furthermore, positive standard anomalies (Figs. 4f–j) remain relatively consistent (at days 5 and 20), although as stated above, as successively poleward latitudes are included, height anomalies tend more positively (Figs. 4h–j).

In addition to these five latitudinal bands at the 500-hPa level, height anomalies at 300 and 700 hPa were also considered for phase 3 in December. Those anomalies (Fig. 5) show similar tendencies across all three vertical

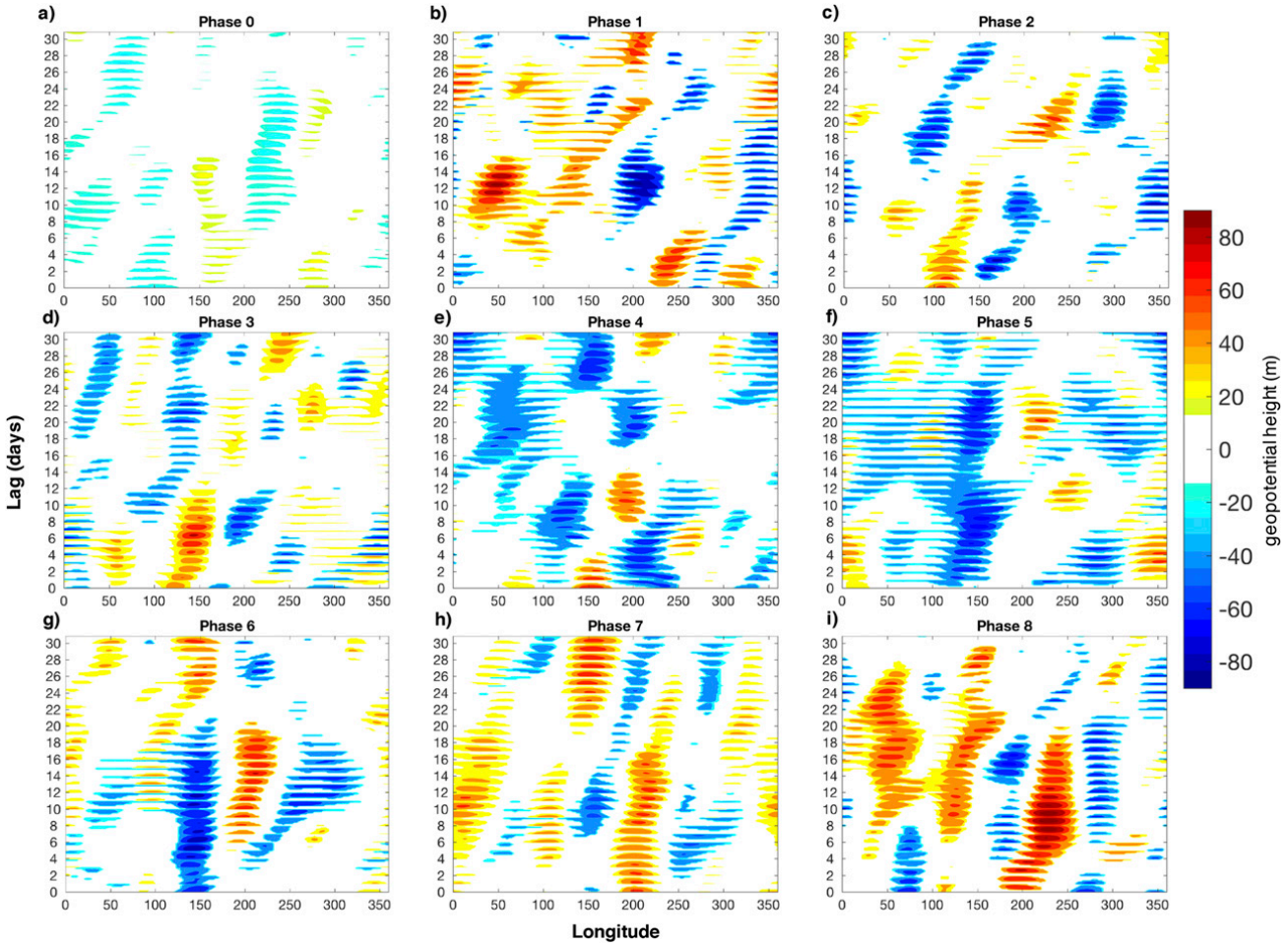

FIG. 6. Hovmöller of December mean geopotential height anomalies at 500 hPa (m), where each of the 31 strips of the *y* axis is the latitudinal band 50°–65°S for all longitudes at 0–30-day temporal lags. MJO phases (a) 0, (b) 1, (c) 2, (d) 3, (e) 4, (f) 5, (g) 6, (h) 7, and (i) 8, where phase 0 refers to inactive MJO occurrences. Lagged anomalies are stacked vertically in each panel, with time increasing along the *y* axis, such that the anomalies at 50°S for one time step are located adjacent to the anomalies at 65°S for the following time step. Only height anomalies statistically significantly different from zero at the 95% level are shown. Sample size for each phase is given in Fig. 2.

levels of the troposphere. For example, clear anomaly peaks at all three tropospheric levels are evident at temporal lags of approximately 5 and 20 days after MJO phase 3. This tendency is present in both positive and negative standard anomalies, with both magnitude and lag of anomalies similar at all three atmospheric levels. This result suggests that the association between the MJO and the Antarctic atmosphere occurs coherently between 700 and 300 hPa, which is consistent with quasi- and semigeostrophic adjustment of a barotropic atmosphere to Rossby wave disturbances (Carlson 1991; Bluestein 1992).

c. *Spatiotemporal variability of the MJO–Antarctic atmosphere relationship*

The next step to better understand associations between the MJO and the Antarctic atmosphere was to analyze the lagged spatiotemporal variability of 500-hPa geopotential height anomalies in the 50°–65°S latitudinal band over 30 days for both June and December. During December, statistically significant (at the 95th percentile) height anomalies tend to organize into an approximate wavenumber-4 pattern (Fig. 6). Phases 6, 7, and 8, in particular, display alternating positive and negative regions of standard anomalies in wavenumber 4, with minimal eastward longitudinal progression over most of the 30-day period. Those patterns are associated with MJO convection in the Western Hemisphere and western Pacific. The tendency of height anomalies after phases 6–8 to remain over the same approximate longitudes is suggestive that MJO convection is associated with a blocking-type circulation pattern in the higher latitudes (e.g., Oliveira et al. 2014). This is particularly evident after phase 7, where positive height anomalies tend to center around 0°, 100°, 210°, and 290° longitude (supporting a wavenumber-4 anomaly pattern) (Figs. 7a–d) and move slowly for

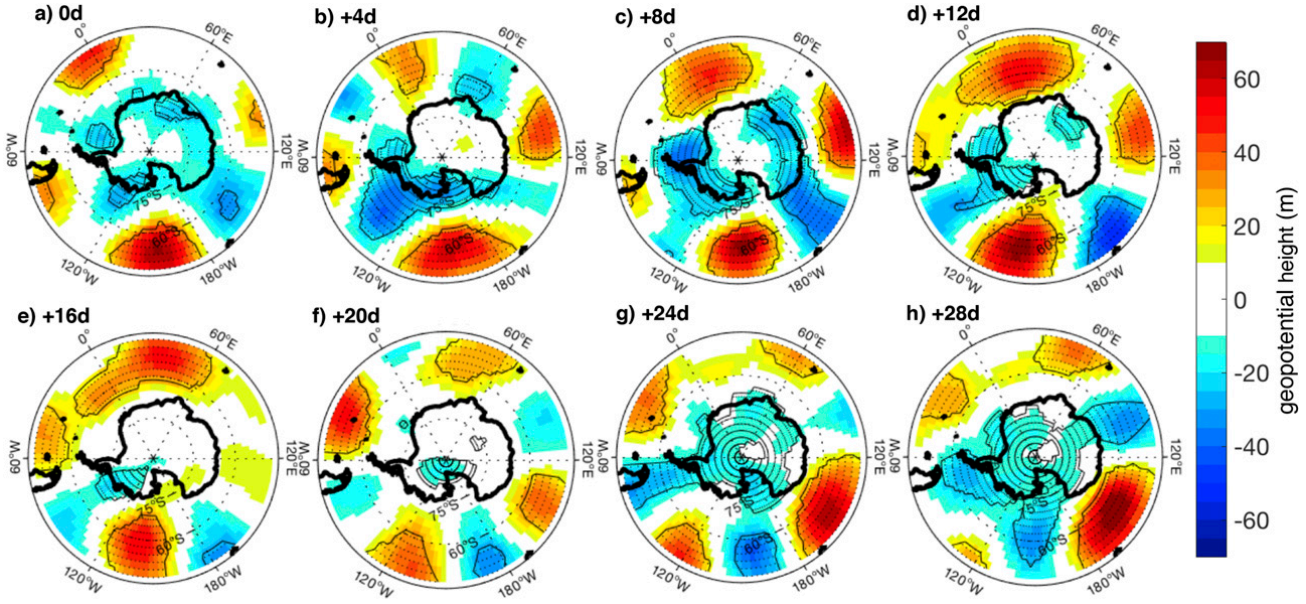

FIG. 7. Geopotential height anomalies at 500 hPa (m) at 4-day lag intervals (a)–(h) from lag 0 to 28 for MJO phase 7in December. Significance at the 95% level is indicated by the stippled areas. Each lag comprises 55 days. Sample size for each phase is given in Fig. 3.

0–12 days after phase 7. This was seen in Fig. 3g, with consistent positive standard anomalies from days 0 to 12. Those anomaly centers then tend to exhibit eastward progression 14–28 days after phase 7 (Figs. 7e–h) and weaken, in agreement with the decline in positive standard anomalies seen in Fig. 3g. In contrast to phases 6–8, phases 3–5 (when MJO convection is over the Indian Ocean and Maritime Continent) show weaker and more progressive, eastward-moving anomaly centers. Finally, near-zero anomalous height values are evident after inactive MJO (phase 0) events.

In comparison with December, the geographical pattern of time-lagged June height anomalies by MJO phase tends toward wavenumber 3 (Fig. 8), which is one wavenumber lower than in December. Additionally, in contrast to the persistent anomaly locations with little eastward progression in December, June height anomalies tend to organize into progressive centers that traverse up to 200° longitude over the 30-day period following MJO convection. This is particularly evident after phase 6 (when convection is centered over the western Pacific Ocean) (Fig. 8i). A positive anomaly center at approximately 160° slowly develops from days 0 to 4 (Figs. 9a,b), grows larger by day 8 (Fig. 9c), and begins progressing eastward through days 12–16 (Figs. 9d,e), reaching 300° by day 28 (Fig. 9h).

4. Summary and conclusions

The goal of this study was to further examine the time-lagged response of Southern Hemisphere tropospheric circulation to tropical MJO forcing, with specific focus on the mid- to high-latitudinal belt associated with some of the strongest variability of the Antarctic atmosphere. The major findings are as follows. First, height anomalies in the Antarctic atmosphere lag convection associated with the Madden–Julian oscillation by up to 30 days. The time lag with strongest height anomalies depends on both the location of the MJO convection (e.g., the MJO phase) and the season. For example, in austral summer, peaks in 500-hPa height anomalies from 5 to 7 days, and again from 15 to 20 days, occur after convection over the Indian Ocean (phases 2 and 3; Fig. 3). The latter of these two identified temporal lags (15–20 days) supports previous work by Fauchereau et al. (2016). However, in austral winter, peaks in 500-hPa height anomalies after convection over the Indian Ocean (phases 2 and 3) occur after 3–5 days, and again after 25 days (Fig. 2). The second major result is that lagged height anomalies in the Antarctic atmosphere are fairly consistent across different vertical levels (e.g., anomaly patterns at 300, 500, and 700 hPa resembled one another) and latitudinal bands (e.g., anomaly patterns at different bands from 45° to 80°S resembled one another). The third major result is that lagged height anomalies after phases 6–8 in December (when the active MJO extends from the western Pacific into the Western Hemisphere) resembled blocking patterns, with anomaly centers in an approximate wavenumber-4 arrangement. Because troposphere blocking patterns have significant implications for weather, and particularly for extreme weather, in the Antarctic and Southern

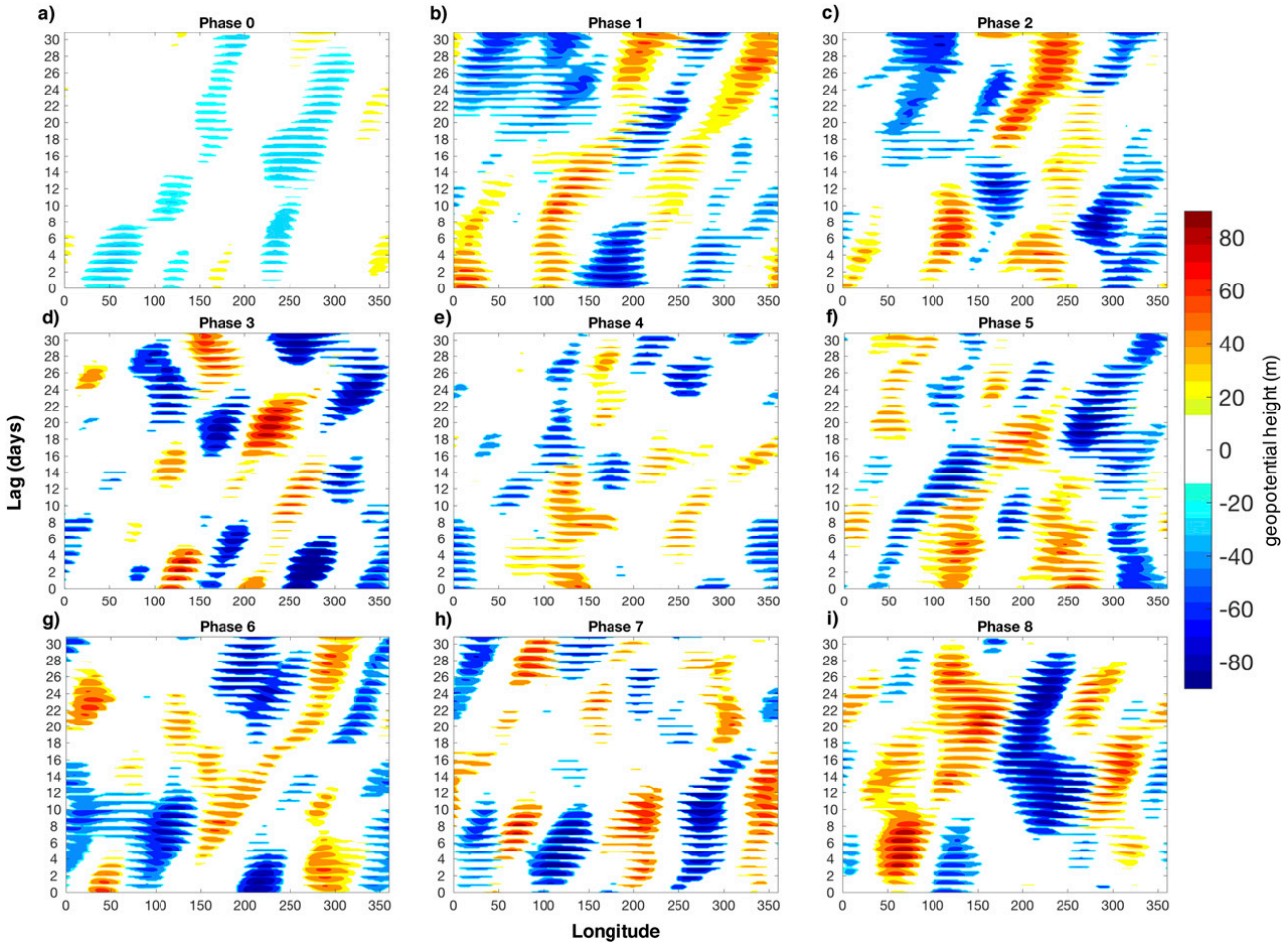

FIG. 8. As in Fig. 6, but for June. Sample size for each phase is given in Fig. 2.

Hemisphere (Trenberth and Mo 1985; Massom et al. 2004; Massom et al. 2006; Berrisford et al. 2007; Pook et al. 2013; Damião Mendes and Cavalcanti 2014; Oliveira et al. 2014), this association between blocking and the MJO is particularly important. Other phases in December (e.g., phases 1–4, when convection extends

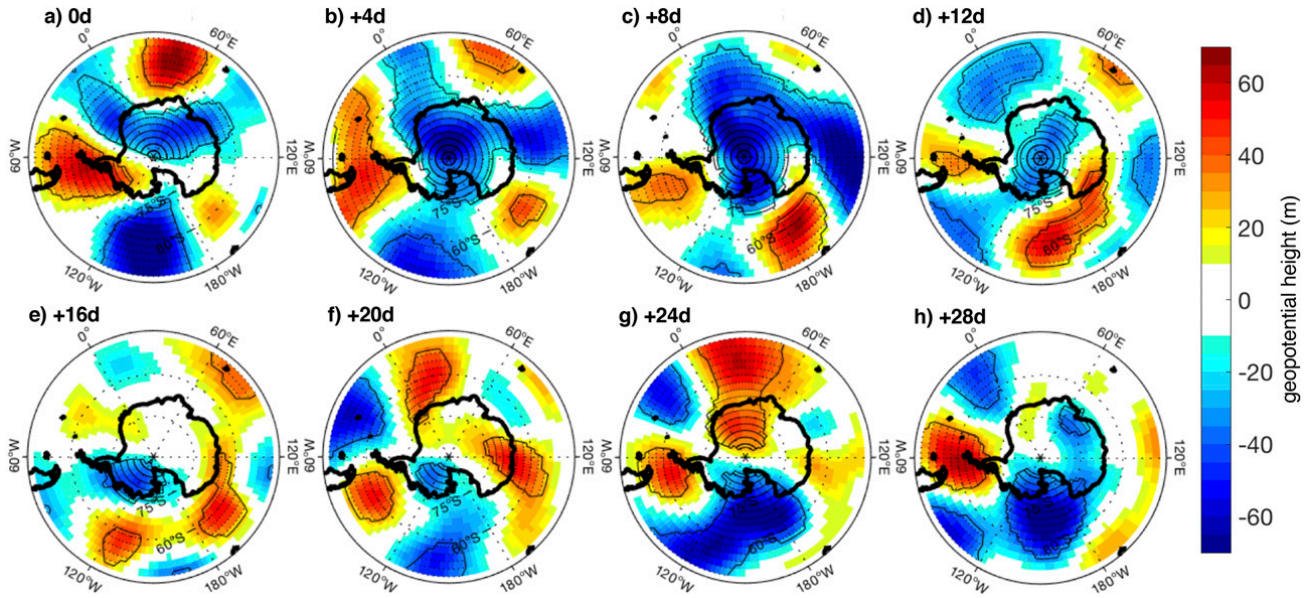

FIG. 9. As in Fig. 7, but for June. Each lag comprises 105 days.

from the Indian Ocean into the Maritime Continent) tend to be associated with more eastward-progressive height anomaly patterns. In June, phases 1–4 tend also to be associated with anomaly patterns that generally progress eastward. However, blocking was evident for up to 10 days after phases 5–7 (when convection is over the Maritime Continent and western Pacific Ocean), and after phase 8 (when the MJO is active over the Western Hemisphere), a blocking pattern from days 15 to 30 develops over much of the South Pacific from 100° to 250°.

It is important to note that the current study focuses on the association between active MJO and subsequent atmospheric height tendencies in the Antarctic troposphere. The height anomalies are identified via atmospheric composites, and while they are often statistically significantly at and beyond the 95th percentile, this study did not examine the pathway between the tropics and extratropics, nor did it explore the complex dynamics of how the association between the MJO and the Antarctic atmosphere evolved. One possible way to explore attribution, and one that is suggested for future work, is to use idealized general circulation models to place MJO-like diabatic heat sources in the tropics and see how the extratropics respond. Another extension of this work would be to explore the cumulative impacts of both MJO and ENSO on Southern Hemisphere extratropical geopotential heights and circulation.

Acknowledgments. This research was partially supported by National Science Foundation Awards ARC-1203843 and AGS-1240143, NASA Award NNX16AH61G, and Office of Naval Research Grant N0001416WX01752.

REFERENCES

Barrett, B. S., J. F. Carrasco, and A. P. Testino, 2012: Madden–Julian oscillation (MJO) modulation of atmospheric circulation and Chilean winter precipitation. *J. Climate*, **25**, 1678–1688, https://doi.org/10.1175/JCLI-D-11-00216.1.

——, G. R. Henderson, and J. S. Werling, 2015: The influence of MJO on the intraseasonal variability of Northern Hemisphere spring snow depth. *J. Climate*, **28**, 7250–7262, https://doi.org/10.1175/JCLI-D-15-0092.1.

Berbery, E. H., and J. Nogues-Paegle, 1993: Intraseasonal fluctuations between the Tropics and extratropics in the Southern Hemisphere. *J. Atmos. Sci.*, **50**, 1950–1965, https://doi.org/10.1175/1520-0469(1993)050<1950:IIBTTA>2.0.CO;2.

Berrisford, P., B. J. Hoskins, and E. Tyrlis, 2007: Blocking and Rossby wave breaking on the dynamical tropopause in the Southern Hemisphere. *J. Atmos. Sci.*, **64**, 2881–2898, https://doi.org/10.1175/JAS3984.1.

Bladé, I., and D. L. Hartmann, 1995: The linear and nonlinear extratropical response to tropical intraseasonal heating. *J. Atmos. Sci.*, **52**, 4448–4471, https://doi.org/10.1175/1520-0469(1995)052<4448:TLANER>2.0.CO;2.

Bluestein, H., 1992: *Synoptic-Dynamic Meteorology in Midlatitudes: Principles of Kinematics and Dynamics*. Oxford University Press, 448 pp.

Branstator, G. W., 2002: Circumglobal teleconnections, the jet stream waveguide, and the North Atlantic Oscillation. *J. Climate*, **15**, 1893–1910, https://doi.org/10.1175/1520-0442(2002)015<1893:CTTJSW>2.0.CO;2.

Carlson, T. N., 1991: *Mid-latitude Weather Systems*. Harper Collins Academic, 507 pp.

Carvalho, L. M., C. Jones, and T. Ambrizzi, 2005: Opposite phases of the Antarctic Oscillation and relationships with intraseasonal to interannual activity in the tropics during the austral summer. *J. Climate*, **18**, 702–718, https://doi.org/10.1175/JCLI-3284.1.

Cassou, C., 2008: Intraseasonal interaction between the Madden-Julian Oscillation and the North Atlantic Oscillation. *Nature,* **455**, 523–527, https://doi.org/10.1038/nature07286.

Damião Mendes, M. C. D., and I. F. A. Cavalcanti, 2014: The relationship between the Antarctic oscillation and blocking events over the South Pacific and Atlantic Oceans. *Int. J. Climatol.*, **34**, 529–544, https://doi.org/10.1002/joc.3729.

Donald, A., H. Meinke, B. Power, A. H. N. de Maia, M. C. Wheeler, N. White, R. C. Stone, and J. Ribbe, 2006: Near-global impact of the Madden-Julian oscillation on rainfall. *Geophys. Res. Lett.*, **33**, L09704, https://doi.org/10.1029/2005GL025155.

Fauchereau, N. N., B. B. Pohl, and A. A. Lorrey, 2016: Extratropical impacts of the Madden–Julian Oscillation over New Zealand from a weather regime perspective. *J. Climate*, **29**, 2161–2175, https://doi.org/10.1175/JCLI-D-15-0152.1.

Ferranti, L., T. N. Palmer, F. Molteni, and K. Klinker, 1990: Tropical–extratropical interaction associated with the 30–60 day oscillation and its impact on medium and extended range prediction. *J. Atmos. Sci.*, **47**, 2177–2199, https://doi.org/10.1175/1520-0469(1990)047<2177:TEIAWT>2.0.CO;2.

Flatau, M., and Y.-J. Kim, 2013: Interaction between the MJO and polar circulations. *J. Climate*, **26**, 3562–3574, https://doi.org/10.1175/JCLI-D-11-00508.1.

Gong, D.-Y., and S.-W. Wang, 1998: Antarctic oscillation: Concept and applications. *Chin. Sci. Bull.*, **43**, 734–738, https://doi.org/10.1007/BF02898949.

——, and ——, 1999: Definition of Antarctic oscillation index. *Geophys. Res. Lett.*, **26**, 459–462, https://doi.org/10.1029/1999GL900003.

Guan, B., D. E. Waliser, N. P. Molotch, E. J. Fetzer, and P. J. Neiman, 2012: Does the Madden–Julian oscillation influence wintertime atmospheric rivers and snowpack in the Sierra Nevada? *Mon. Wea. Rev.*, **140**, 325–342, https://doi.org/10.1175/MWR-D-11-00087.1.

Henderson, G. R., B. S. Barrett, and D. M. LaFleur, 2014: Arctic sea ice and the Madden-Julian Oscillation (MJO). *Climate Dyn.*, **43**, 2185–2196, https://doi.org/10.1007/s00382-013-2043-y.

Henderson, S. A., E. D. Maloney, and E. A. Barnes, 2016: The influence of the Madden–Julian Oscillation on Northern Hemisphere winter blocking. *J. Climate*, **29**, 4597–4616, https://doi.org/10.1175/JCLI-D-15-0502.1.

Hendon, H. H., B. Liebmann, M. Newman, J. D. Glick, and J. E. Schemm, 2000: Medium-range forecast errors associated with active episodes of the Madden–Julian oscillation. *Mon. Wea. Rev.*, **128**, 69–86, https://doi.org/10.1175/1520-0493(2000)128<0069:MRFEAW>2.0.CO;2.

Higgins, R. W., J.-K. E. Schemm, W. Shi, and A. Leetmaa, 2000: Extreme precipitation events in the western United States

related to tropical forcing. *J. Climate*, **13**, 793–820, https://doi.org/10.1175/1520-0442(2000)013<0793:EPEITW>2.0.CO;2.

Hoskins, B., and D. Karoly, 1981: The steady linear response of a spherical atmosphere to thermal and orographic forcing. *J. Atmos. Sci.*, **38**, 1179–1196, https://doi.org/10.1175/1520-0469(1981)038<1179:TSLROA>2.0.CO;2.

Jacques-Coper, M., S. Brönnimann, O. Martius, C. S. Vera, and S. B. Cerne, 2015: Evidence for a modulation of the intraseasonal summer temperature in eastern Patagonia by the Madden–Julian Oscillation. *J. Geophys. Res. Atmos.*, **120**, 7340–7357, https://doi.org/10.1002/2014JD022924.

Jin, F., and B. J. Hoskins, 1995: The direct response to tropical heating in a baroclinic atmosphere. *J. Atmos. Sci.*, **52**, 307–319, https://doi.org/10.1175/1520-0469(1995)052<0307:TDRTTH>2.0.CO;2.

Jones, C., D. E. Waliser, K. M. Lau, and W. Stern, 2004: The Madden–Julian oscillation and its impact on Northern Hemisphere weather predictability. *Mon. Wea. Rev.*, **132**, 1462–1471, https://doi.org/10.1175/1520-0493(2004)132<1462:TMOAII>2.0.CO;2.

——, A. Hazra, and L. M. V. Carvalho, 2015: The Madden–Julian oscillation and boreal winter forecast skill: An analysis of NCEP CFSv2 reforecasts. *J. Climate*, **28**, 6297–6307, https://doi.org/10.1175/JCLI-D-15-0149.1.

Kanamitsu, M., W. Ebisuzaki, J. Woollen, S.-K. Yang, J. J. Hnilo, M. Fiorino, and G. L. Potter, 2002: NCEP-DOE AMIP-II Reanalysis (R-2). *Bull. Amer. Meteor. Soc.*, **83**, 1631–1643, https://doi.org/10.1175/BAMS-83-11-1631.

Kiladis, G. N., and K. M. Weickmann, 1992a: Circulation anomalies associated with tropical convection during northern winter. *Mon. Wea. Rev.*, **120**, 1900–1923, https://doi.org/10.1175/1520-0493(1992)120<1900:CAAWTC>2.0.CO;2.

——, and ——, 1992b: Extratropical forcing of tropical Pacific convection during northern winter. *Mon. Wea. Rev.*, **120**, 1924–1938, https://doi.org/10.1175/1520-0493(1992)120<1924:EFOTPC>2.0.CO;2.

——, and ——, 1997: Horizontal structure and seasonality of large-scale circulations associated with submonthly tropical convection. *Mon. Wea. Rev.*, **125**, 1997–2013, https://doi.org/10.1175/1520-0493(1997)125<1997:HSASOL>2.0.CO;2.

Lafleur, D. M., B. S. Barrett, and G. R. Henderson, 2015: Some climatological aspects of the Madden–Julian Oscillation (MJO). *J. Climate*, **28**, 6039–6053, https://doi.org/10.1175/JCLI-D-14-00744.1.

L'Heureux, M. L., and R. Higgins, 2008: Boreal winter links between the Madden–Julian oscillation and the Arctic Oscillation. *J. Climate*, **21**, 3040–3050, https://doi.org/10.1175/2007JCLI1955.1.

Li, W., W. Guo, P. Hsu, and Y. Xue, 2016: Influence of the Madden–Julian oscillation on Tibetan Plateau snow cover at the intraseasonal time-scale. *Sci. Rep.*, **6**, 30456, https://doi.org/10.1038/srep30456.

Limpasuvan, V., and D. L. Hartmann, 1999: Eddies and the annular modes of climate variability. *Geophys. Res. Lett.*, **26**, 3133–3136, https://doi.org/10.1029/1999GL010478.

Madden, R. A., and P. R. Julian, 1972: Description of global-scale circulation cells in the tropics with a 40–50 day period. *J. Atmos. Sci.*, **29**, 1109–1123, https://doi.org/10.1175/1520-0469(1972)029<1109:DOGSCC>2.0.CO;2.

Massom, R. A., M. J. Pook, J. C. Comiso, N. Adams, J. Turner, T. Lachlan-Cope, and T. Gibson, 2004: Precipitation over the interior East Antarctic Ice Sheet related to mid-latitude blocking-high activity. *J. Climate*, **17**, 1914–1928, https://doi.org/10.1175/1520-0442(2004)017<1914:POTIEA>2.0.CO;2.

——, and Coauthors, 2006: Extreme anomalous atmospheric circulation in the west Antarctic peninsula region in austral spring and summer 2001/02, and its profound impact on sea ice and biota. *J. Climate*, **19**, 3544–3571, https://doi.org/10.1175/JCLI3805.1.

Matthews, A. J., and M. P. Meredith, 2004: Variability of Antarctic circumpolar transport and the Southern Annular Mode associated with the Madden-Julian Oscillation. *Geophys. Res. Lett.*, **31**, L24312, https://doi.org/10.1029/2004GL021666.

Mo, K. C., 2000: Relationships between low-frequency variability in the Southern Hemisphere and sea surface temperature anomalies. *J. Climate*, **13**, 3599–3610, https://doi.org/10.1175/1520-0442(2000)013<3599:RBLFVI>2.0.CO;2.

——, and R. W. Higgins, 1998a: Tropical influences on California precipitation. *J. Climate*, **11**, 412–430, https://doi.org/10.1175/1520-0442(1998)011<0412:TIOCP>2.0.CO;2.

——, and ——, 1998b: The Pacific–South American modes and tropical convection during the Southern Hemisphere winter. *Mon. Wea. Rev.*, **126**, 1581–1596, https://doi.org/10.1175/1520-0493(1998)126<1581:TPSAMA>2.0.CO;2.

Moore, R. W., O. Martius, and T. Spengler, 2010: The modulation of the subtropical and extratropical atmosphere in the Pacific basin in response to the Madden–Julian oscillation. *Mon. Wea. Rev.*, **138**, 2761–2779, https://doi.org/10.1175/2010MWR3194.1.

Paegle, J. N., L. A. Byerle, and K. C. Mo, 2000: Intraseasonal modulation of South American summer precipitation. *Mon. Wea. Rev.*, **128**, 837–850, https://doi.org/10.1175/1520-0493(2000)128<0837:IMOSAS>2.0.CO;2.

Oliveira, F. N., L. Carvalho, and T. Ambrizzi, 2014: A new climatology for Southern Hemisphere blockings in the winter and the combined effect of ENSO and SAM phases. *Int. J. Climatol.*, **34**, 1676–1692, https://doi.org/10.1002/joc.3795.

Pook, M. J., J. S. Risbey, P. C. McIntosh, C. C. Ummenhofer, A. G. Marshall, and G. A. Meyers, 2013: The seasonal cycle of blocking and associated physical mechanisms in the Australian region and relationship with rainfall. *Mon. Wea. Rev.*, **141**, 4534–4553, https://doi.org/10.1175/MWR-D-13-00040.1.

Renwick, J. A., and M. J. Revell, 1999: Blocking over the South Pacific and Rossby wave propagation. *Mon. Wea. Rev.*, **127**, 2233–2247, https://doi.org/10.1175/1520-0493(1999)127<2233:BOTSPA>2.0.CO;2.

Roundy, P. E., 2012: Tropical-extratropical interactions. *Intraseasonal Variability of the Atmosphere–Ocean Climate System*, 2nd ed. W. K.-M. Lau and D. E. Waliser, Eds., Springer, 497–512.

——, C. J. Schreck III, and M. A. Janiga, 2009: Contributions of convectively coupled equatorial Rossby waves and Kelvin waves to the real-time multivariate MJO indices. *Mon. Wea. Rev.*, **137**, 469–478, https://doi.org/10.1175/2008MWR2595.1.

Sardeshmukh, P. D., and B. J. Hoskins, 1988: The generation of global rotational flow by steady idealized tropical divergence. *J. Atmos. Sci.*, **45**, 1228–1251, https://doi.org/10.1175/1520-0469(1988)045<1228:TGOGRF>2.0.CO;2.

Schreck, C. J., J. M. Cordeira, and D. Margolin, 2013: Which MJO events affect North American temperatures? *Mon. Wea. Rev.*, **141**, 3840–3850, https://doi.org/10.1175/MWR-D-13-00118.1.

Seo, K.-H., and S.-W. Son, 2012: The global atmospheric circulation response to tropical diabatic heating associated with the Madden–Julian oscillation during northern winter. *J. Atmos. Sci.*, **69**, 79–96, https://doi.org/10.1175/2011JAS3686.1.

——, H. Lee, and D. W. Frierson, 2016: Unraveling the teleconnection mechanisms that induce wintertime temperature

anomalies over the Northern Hemisphere continents in response to the MJO. *J. Atmos. Sci.*, **73**, 3557–3571, https://doi.org/10.1175/JAS-D-16-0036.1.

Sobel, A., and E. Maloney, 2013: Moisture modes and the eastward propagation of the MJO. *J. Atmos. Sci.*, **70**, 187–192, https://doi.org/10.1175/JAS-D-12-0189.1.

Straub, K. H., 2013: MJO initiation in the real-time multivariate MJO index. *J. Climate*, **26**, 1130–1151, https://doi.org/10.1175/JCLI-D-12-00074.1.

Sun, X. J., P. X. Wang, and J. X. L. Wang, 2017: An assessment of the atmospheric centers of action in the northern hemisphere winter. *Climate Dyn.*, **48**, 1031–1047, https://doi.org/10.1007/s00382-016-3126-3.

Trenberth, K. E., and K. C. Mo, 1985: Blocking in the Southern Hemisphere. *Mon. Wea. Rev.*, **113**, 3–21, https://doi.org/10.1175/1520-0493(1985)113<0003:BITSH>2.0.CO;2.

Vecchi, G. A., and N. A. Bond, 2004: The Madden-Julian Oscillation (MJO) and northern high latitude wintertime surface air temperatures. *Geophys. Res. Lett.*, **31**, L04104, https://doi.org/10.1029/2003GL018645.

Ventrice, M. J., C. D. Thorncroft, and P. E. Roundy, 2011: The Madden–Julian oscillation's influence on African easterly waves and downstream tropical cyclogenesis. *Mon. Wea. Rev.*, **139**, 2704–2722, https://doi.org/10.1175/MWR-D-10-05028.1.

——, M. C. Wheeler, H. H. Hendon, C. J. Schreck III, C. D. Thorncroft, and G. N. Kiladis, 2013: A modified multivariate Madden–Julian oscillation index using velocity potential. *Mon. Wea. Rev.*, **141**, 4197–4210, https://doi.org/10.1175/MWR-D-12-00327.1.

Wallace, J. M., and D. S. Gutzler, 1981: Teleconnections in the geopotential height field during the Northern Hemisphere winter. *Mon. Wea. Rev.*, **109**, 784–812, https://doi.org/10.1175/1520-0493(1981)109<0784:TITGHF>2.0.CO;2.

Weickmann, K. M., and E. Berry, 2007: A synoptic–dynamic model of subseasonal atmospheric variability. *Mon. Wea. Rev.*, **135**, 449–474, https://doi.org/10.1175/MWR3293.1.

——, G. N. Kiladis, and P. D. Sardeshmukh, 1997: The dynamics of intraseasonal atmospheric angular momentum oscillations. *J. Atmos. Sci.*, **54**, 1445–1461, https://doi.org/10.1175/1520-0469(1997)054<1445:TDOIAA>2.0.CO;2.

Wheeler, M. C., and H. H. Hendon, 2004: An all-season real-time multivariate MJO index: Development of an index for monitoring and prediction. *Mon. Wea. Rev.*, **132**, 1917–1932, https://doi.org/10.1175/1520-0493(2004)132<1917:AARMMI>2.0.CO;2.

Zhang, C., 2005: Madden-Julian Oscillation. *Rev. Geophys.*, **43**, RG2003, https://doi.org/10.1029/2004RG000158.

——, 2013: Madden–Julian Oscillation: Bridging weather and climate. *Bull. Amer. Meteor. Soc.*, **94**, 1849–1870, https://doi.org/10.1175/BAMS-D-12-00026.1.

Zhou, S., and A. J. Miller, 2005: The interaction of the Madden–Julian Oscillation and the Arctic Oscillation. *J. Climate*, **18**, 143–159, https://doi.org/10.1175/JCLI3251.1.

Zhou, Y., Y. Lu, B. Yang, J. Jiang, A. Huang, Y. Zhao, M. La, and Q. Yang, 2016: On the relationship between the Madden-Julian Oscillation and 2 m air temperature over central Asia in boreal winter. *J. Geophys. Res. Atmos.*, **121**, 13,250–13,272, https://doi.org/10.1002/2016JD025651.